

## Machine failure forewarning via phase-space dissimilarity measures

L. M. Hively and V. A. Protopopescu

*Oak Ridge National Laboratory, Oak Ridge, Tennessee 37831*

(Received 23 October 2003; accepted 18 January 2004; published online 21 May 2004)

We present a model-independent, data-driven approach to quantify dynamical changes in nonlinear, possibly chaotic, processes with application to machine failure forewarning. From time-windowed data sets, we use time-delay phase-space reconstruction to obtain a discrete form of the invariant distribution function on the attractor. Condition change in the system's dynamic is quantified by dissimilarity measures of the difference between the test case and baseline distribution functions. We analyze time-serial mechanical (vibration) power data from several large motor-driven systems with accelerated failures and seeded faults. The phase-space dissimilarity measures show a higher consistency and discriminating power than traditional statistical and nonlinear measures, which warrants their use for timely forewarning of equipment failure. © 2004 American Institute of Physics. [DOI: 10.1063/1.1667631]

One of the most important problems in time-series analysis is the suitable characterization of system dynamics for timely, accurate, and robust condition assessment. In particular, timely forewarning of failures in machinery and industrial equipment is essential to avoid down-time, costly repairs, and—possibly—catastrophic events. Machine processes display complex, nonstationary, and noisy behaviors that may range from (quasi-)periodic to completely irregular (chaotic) regimes. Even when their behavior becomes very irregular (e.g., tool chatter), it is reasonable to assume that—for all practical purposes—most of these systems have low dimensionality. As a result, analysis of their dynamical features can be done via traditional nonlinear measures (TNM), such as Lyapunov exponents, Kolmogorov entropy, and correlation dimension. While these measures are adequate for discriminating between clear-cut regular and chaotic dynamics, they are not sufficiently sensitive to distinguish between slightly different chaotic regimes, especially when the data are noisy and/or limited. Typically, machine dynamics fall into this latter category, creating a massive roadblock to failure prognostication. To address this problem, we developed a new approach that is better suited to capture changes in the underlying dynamics. We start from robust process-indicative data, recognizing that some data capture the full richness of the dynamics while other data may not. The data are checked for quality, and inadequate data (e.g., lost data points, intervals with unchanged signal amplitude, low sampling rate, excessive periodic content, excessive noise, saturation at high or low limits, and inconsistent signal amplitude across datasets in the test sequence) are not analyzed. Acceptable data are filtered to remove confounding artifacts (e.g., sinusoidal variation in three-phase electrical signals), and the artifact-filtered time-serial data are then used to recover the essential features of the dynamics via standard time-delay phase-space reconstruction. One result of this reconstruction of the underlying dynamics is a discrete approximation of the distribution function (DF)

on the attractor. If the dynamical state is unaltered, the geometry of the attractor and the visitation frequencies of its various points do not change. This DF represents the baseline. Condition change is established by comparing the baseline DF to subsequent test-case DFs via new measures of dissimilarity, namely the  $L_1$  distance and  $\chi^2$  statistic between two DFs. A clear trend in the dissimilarity measures over time indicates substantial departure from the baseline dynamics, thus signaling condition change. Depending on its severity, this departure also can be interpreted as forewarning of an impending failure. We illustrate this approach on triaxial acceleration data from machinery tests for seeded faults and accelerated failures. Our method yields robust nonlinear signatures of degradation and its progression, allowing earlier and more accurate detection of the machine failure in comparison to TNM.

### I. INTRODUCTION

Condition-based (predictive) maintenance relies heavily on failure prognostication, based on analysis of machine data. The major roadblocks to accurate, timely, and robust prognostication include:<sup>1</sup> (a) incomplete understanding of fault evolution and failure physics; (b) lack of predictive methodologies for unsteady failure signatures; (c) ignorance about controlling parameters; and (d) unavailability of test facilities to emulate a real operating environment. Our present approach is far from proposing a complete and universally applicable solution to this problem, but does offer a partial solution. In particular, we address items (a)–(b) by quantifying the (nonstationary) condition change as a sequence of nonlinear statistical signatures; item (c) by associating change in the controlling parameter with the equipment response; and item (d) by designing, running, and analyzing tests that are similar to in-plant operations.

Machine dynamics<sup>2–27</sup> has a long history.<sup>11</sup> Metal cutting forces during machine tool chatter have long been recognized as “very complex” and “very far from sinusoidal,”

implying nonlinear dynamics.<sup>23</sup> Tlustý<sup>12,18,20</sup> published extensive experimental (in)stability diagrams for turning, milling, boring, hobbing, and planing. Qu *et al.*<sup>16</sup> used nonlinear measures to diagnose dynamics, using vibration data from rotating machinery (turbogenerator and compressor). Bukkapatnam *et al.*<sup>3</sup> analyzed data from lathe cutting and found low dimensional, chaotic features. Our previous work analyzed the nonlinear dynamics of machine tool chatter,<sup>28,29</sup> and used phase-space (PS) dissimilarity to detect condition change in various physical processes, namely, distinguishing different drilling conditions (tool wear) from spindle motor current of a machining center; distinguishing (un)balanced centrifugal pump states from electrical motor power; and forewarning of a bellows coupling failure in a rotating drive train from motor current.<sup>30</sup> Our more recent work used phase-space dissimilarity to determine condition change in machines due to seeded faults and accelerated failure progression.<sup>31,32,34</sup> Delogu, Rustici, and co-workers found hyperchaos<sup>35</sup> and intermittent chaos<sup>36</sup> in ball milling. Pfeiffer's analysis<sup>37</sup> showed that bifurcations and chaos may be generated by various mechanical processes, such as stick-slip due to dynamic/static friction and surface impacts; additional processes include surface deformation and material removal/wear.<sup>12,18,20</sup>

To date, most of the effort on condition change assessment and forewarning has focused on Fourier spectra, conventional statistical measures (CSM), and traditional nonlinear measures (TNM), such as Kolmogorov entropy, correlation dimension, and Lyapunov exponents. While these descriptors discriminate adequately between clear-cut regular and chaotic dynamics,<sup>38-41</sup> they are not always sufficiently sensitive to distinguish between slightly different chaotic regimes, especially when data are limited and/or noisy. Indeed, our initial analysis of machine data<sup>28</sup> used TNM, yielding inconsistent detection and event forewarning. Those results indicated that detection of meaningful information in attenuated, noisy, artifact-infested signals requires more sensitive and discriminating measures. Our more recent work showed by direct comparison that phase-space dissimilarity measures (PSDM) have consistently better sensitivity and discrimination power for event forewarning than TNM.<sup>30,31</sup>

The remainder of this paper is organized as follows. Section II reviews our methodology, using various measures for time series analysis: CSM, TNM, and PSDM. Moreover, we present the details of a recently developed<sup>32</sup> statistical test for failure forewarning and onset. Section III presents our results for various machine data. Section IV summarizes the results and presents our conclusions.

## II. APPROACH

Machine processes display rich dynamics, including quasiperiodicity, nonlinearity, and occasional chaos. Using recent advances in nonlinear science to capture and interpret such features, our analysis of condition change relies on a few basic assumptions, namely: (i) the underlying machine dynamics are essentially deterministic; (ii) machine processes behave as a low-dimensional nonlinear, possibly chaotic dynamical system; (iii) a single channel of data can cap-

ture the main features of nonlinear dynamics. (Phase-space reconstruction of multichannel data is certainly possible, and is the subject of future work.)

Several practical caveats are also in order. We assume adequate quality data. For example, an insufficient amount of time-serial data does not adequately sample the attractor, thereby degrading the sensitivity of the dissimilarity measures.<sup>42,43</sup> Likewise, the data sampling rate,  $f_s$ , must be much larger than the machine dynamical rate,  $\nu$ , which in turn must be much larger in comparison to the inverse of the time,  $T$ , to failure:  $f_s \gg \nu \gg 1/T$ . We assure the validity of this assumption by requiring that the first minimum in the mutual information function occur at four (or more) time steps, where one time step corresponds to  $\tau=1$  fs. Usually, the analysis is confounded by artifacts in the data. Based on *a priori* information about the underlying dynamics, we remove such artifacts, such as sinusoidal variation in three-phase electrical power or resonant oscillations in vibration power. Also, parameters for the phase-space reconstruction must be chosen carefully for robust and sensitive indication of condition change. This part of the methodology is still too analyst-intensive to be implementable on an industrial scale; practical prognostication must be less dependent on interaction with or guidance from the human expert. Finally, the applicability of the present methodology is limited to *retrospective* analysis of *archival* data for seeded faults and accelerated failures, which are well characterized under appropriate test conditions. A practical application of this approach will require *prospective* analysis of (*near*-)real-time data. The separation between the present state of our methodology and the real-world need is still large and will require substantial additional development.

The general approach is outlined next. We first acquire a process-indicative scalar signal,  $e$ , which is sampled at equal time intervals,  $\tau$ , starting at an initial time,  $t_0$ , yielding a time-serial sequence of  $N$  points,  $e_i = e(t_0 + i\tau)$ . We remove artifacts from the data (e.g., sinusoidal variation in three-phase motor power) with a zero-phase quadratic filter<sup>44,45</sup> that performs better than conventional filters. This filter uses a moving window of  $2w+1$  points of data, with the same number of data points,  $w$ , on either side of a central point. We fit a parabola in the least-squares sense to these data points, and use the central point of the fit to estimate the low-frequency artifact,  $f_i$ . The residual (artifact-filtered) signal,  $g_i = e_i - f_i$ , has essentially no low-frequency artifact activity. All subsequent analysis uses this artifact-filtered data,  $g_i$ .

We convert each artifact-filtered value,  $g_i$ , into a symbolized value,  $s_i$ , namely one of  $S$  different equiprobable integers,  $0, 1, \dots, S-1$ . These symbols are formed by ordering all  $N$  of the base case artifact-filtered time-serial data points from the smallest to largest value. The first  $N/S$  of these ordered values correspond to the first symbol, 0. Ordered data values  $(N/S)+1$  through  $2N/S$  correspond to the second symbol, 1, and so on. Equiprobable symbols have non-uniform partitions in the signal amplitude with the same occurrence frequency of  $g_i$  values by construction, and thus have no information about the PS structure. In contrast, symbols with uniform partitions (uniform symbols) carry inher-

ent dynamical structure prior to the PS reconstruction. Thus, one advantage of equiprobable symbols is that dynamical structure arises *only* from the PS reconstruction, as described below. Moreover, large negative and large positive values of  $g_i$  have little effect on equiprobable symbolization, but dramatically change the partitions for uniform symbols. Information theoretic measures of the PS-DF (e.g., mutual information function) are smooth functions of the reconstruction parameters for equiprobable symbols, but are noisy functions of these same parameters for uniform symbols. For these reasons, equiprobable symbols provide better discrimination of condition change than uniform symbols.

### A. Conventional statistical measures

CSM have long been used for general characterization. The most common statistical measures are the mean:  $\bar{g} = \sum_i g_i / N$ , where the sum over  $i$ ,  $\sum_i$ , spans all  $N$  of the points in the analysis window, and the sample standard deviation,  $\sigma$ , which is  $\sigma^2 = \sum_i (g_i - \bar{g})^2 / (N - 1)$ . Higher moments<sup>46</sup> about the mean include skewness,  $s = \sum_i (g_i - \bar{g})^3 / N\sigma^3$ , and kurtosis,  $k = \sum_i (g_i - \bar{g})^4 / N\sigma^4 - 3$ . A large positive (negative) value of skewness corresponds to a longer, fatter tail in the distribution about the mean to the right (left). Kurtosis measures the amount of flattening ( $k < 0$ ) or excess peakedness ( $k > 0$ ) about the mean. Another measure is the average number of time steps per wave cycle (frequently used in engineering analysis of sampled data),  $m = N / [(n_c - 1) / 2] \approx 2N / n_c$ , for  $n_c \gg 1$ . Here,  $n_c$  is the average number of mean crossings; the two successive mean crossings delimit one-half of a wave period. The position of the first zero in the autocorrelation function, as defined by  $A(j) = \sum_i (g_i - \bar{g})(g_{i+j} - \bar{g}) / (N - j)\sigma^2$ , is also a useful quantity. Nevertheless, while CSM are useful in the analysis of linear processes, they provide inconsistent discrimination for detection of condition change in nonlinear systems. We include them here for completeness and comparison.

### B. Traditional nonlinear measures

The advent and rapid development of nonlinear and chaotic dynamics over the last few decades has produced new and powerful measures for characterization via PS reconstruction,<sup>39,40,47</sup> which uses time-delay vectors that are formed from the artifact-filtered, symbolized data,  $y(i) = [s_i, s_{i+\lambda}, \dots, s_{i+(d-1)\lambda}]$ . The choice of lag,  $\lambda$ , and embedding dimension,  $d$ , determines how well the PS reconstruction unfolds the dynamics. Too high an embedding dimension could result in overfitting of real data with finite length and noise. Moreover, different observables of a system contain unequal amounts of dynamical information,<sup>38</sup> implying that PS reconstruction could be easier from one variable, but more difficult or impossible from another. Our analysis seeks to balance these caveats for finite-length noisy data.

We use the phase, traditional nonlinear measures (TNM), as distinct from the PS measures, as defined in the next subsection. We choose three of the most-frequently-used TNM, as potential indicators of dissimilarity, namely: (i) the first minimum in the mutual information function as a measure of decorrelation time, (ii) the correlation dimension as a measure of complexity, and (iii) the Kolmogorov entropy as a

measure of predictability. We describe these measures next, with more detailed definitions and characterizations in the references cited below.

The mutual information function (MIF) measures average bits of information that can be inferred from one measurement about a second, as a function of the time delay between the two signals. Shannon and Weaver<sup>48</sup> developed the MIF, which was later applied to time series.<sup>49</sup> One set of measurements is  $q = \{q_1, q_2, \dots, q_N\}$ , with associated occurrence probabilities,  $P(q_1), P(q_2), \dots, P(q_N)$ . A second set of measurements is  $r = \{r_1, r_2, \dots, r_N\}$ , with a time delay relative to  $Q$ , and with occurrence probabilities  $P(r_1), P(r_2), \dots, P(r_N)$ .  $P(q_i, r_j)$  is the joint probability that both states occur simultaneously. The first minimum in the MIF,  $M_1$ , gives an average decorrelation time. Then, the MIF is defined as  $I(q, r) = I(r, q) = H(q) + H(r) - H(r, q)$ , where  $H$  is entropy:  $H(q) = -\sum_i P(q_i) \log_2[P(q_i)]$  and  $H(q, r) = -\sum_i P(q_i, r_j) \log_2[P(q_i, r_j)]$ .

The maximum-likelihood correlation dimension<sup>50,51</sup> is  $D = -M \{ \sum_{ij} \ln[(\delta_{ij}/\delta_0 - \delta_n/\delta_0)/(1 - \delta_n/\delta_0)] \}^{-1}$ , where  $M$  is the number of randomly-sampled pairs of phase-space points. The maximum-norm distance between PS-point pairs,  $i$  and  $j$ , is  $\delta_{ij} = \max(0 \leq k \leq m-1) |g_{i+k} - g_{j+k}|$ , where  $m$  is the average number of data points per cycle, as defined above under CSM. The distance  $\delta_n$  is the scale length that is associated with noise. Distances are normalized with respect to a nominal scale length,  $\delta_0$ , which is chosen to balance between sensitivity to local dynamics (typically at  $\delta_0 \leq 5a$ ) and avoidance of excessive noise (typically at  $\delta_0 \geq a$ ). Here, the symbol  $a$  denotes the absolute average deviation as a robust indicator of variability,<sup>52</sup>  $a = \sum_i |g_i - \bar{g}| / N$ .

The Kolmogorov entropy ( $K$ -entropy),  $K$ , is the rate of information loss per unit time (bits per second), and is the sum of the positive Lyapunov exponents. Positive, finite  $K$  is generally viewed as a clear indication that the process manifests chaotic dynamics. Very large entropy indicates a stochastic (totally unpredictable) phenomenon.  $K$  is estimated from the average number of time steps,  $b_i$ , for two PS points, initially within  $\delta \leq \delta_0$ , to diverge to  $\delta > \delta_0$ . We use the maximum-likelihood form of Schouten *et al.*,<sup>52</sup>  $K = -f_s \log(1 - 1/b)$ , with  $b = \sum_i b_i / M$  for  $M$  point pairs. The data-sampling rate is  $f_s$ .

TNM capture nonlinear features of the underlying process, but do not offer a very sensitive tool for detection of dynamical change. The main reason is that TNM, like CSM, are expressed as a sum (or integral) over (a region of) the PS, which averages all dynamical details into one number. Consequently, two (very) different dynamical regimes may lead to very close, or even equal measures. Moreover, the usual definitions of  $K$ -entropy and correlation dimension are in the limit of zero scale length. However, all real data have noise, and even noiseless model data are limited by the finite precision computations. Thus, we use a finite length scale that is somewhat larger than the noise ( $\delta_0 = 2a$ ), at which to report the values of  $K$  and  $D$ . Consequently, our values of  $K$  and  $D$  do not capture dynamical complexity at length scales smaller than  $\delta_0$  and have smaller values than expected for the zero-scale-length limit ( $\delta_0 \rightarrow 0$ ).

### C. Phase-space dissimilarity measures

To overcome some of the limitations of CSM and TNM as discriminators of condition change, we introduced phase-space dissimilarity measures (PSDM),<sup>30–34</sup> which we review briefly for the reader’s convenience. After reconstructing the dynamics (as discussed above), we use appropriate symbolization (also as described above) to partition the phase-space (PS) into  $S^d$  hypercubes or bins. By counting the number of PS points that occur in each bin, we obtain the distribution function (DF) as a discretized density on the attractor. We denote the population of the  $j$ th DF bin,  $R_j$ , for the base case (nominal state), and  $S_j$  for a test case (off-normal state), respectively. Comparison of the test case to the base case involves measuring the difference between  $R_j$  with  $S_j$  by the  $\chi^2$  statistic and  $L_1$  distance:

$$\chi^2 = \sum_j (R_j - S_j)^2 / (R_j + S_j), \tag{1}$$

$$L = \sum_j |R_j - S_j|. \tag{2}$$

The summations in Eqs. (1)–(2) run over all of the populated PS cells. The  $\chi^2$  statistic is one of the most powerful, robust, and widely used tests for dissimilarity between two DFs. This  $\chi^2$  is not an unbiased statistic for accepting or rejecting a null statistical hypothesis,<sup>45</sup> but rather is a measure of dissimilarity between the two DFs. The  $L_1$  distance is the natural metric for DFs by its direct relation to the total invariant measure on the attractor. These measures account for changes in the geometry and visitation frequency of the attractor. Consistent calculation obviously requires the same number of points in both the base case and test case DFs, identically sampled; otherwise the distribution functions must be properly rescaled.

The accuracy and sensitivity of the PS reconstruction can be enhanced by connecting successive PS points as prescribed by the underlying dynamics,  $y(i) \rightarrow y(i+1)$ . Thus, we obtain a discrete representation of the process flow<sup>39,40</sup> as a  $2d$ -dimensional, connected-phase-space (CPS) vector,  $Y(i) = [y(i), y(i+1)]$ , that is formed by adjoining two successive vectors from the  $d$ -dimensional reconstructed PS. As before,  $R$  and  $S$  denote the CPS DFs for the base case and test case, respectively. We then define the measures of dissimilarity between these two CPS DFs via the  $L_1$ -distance and  $\chi^2$  statistic, as before<sup>42,43,53–55</sup>

$$\chi_c^2 = \sum_{jk} (R_{jk} - S_{jk})^2 / (R_{jk} + S_{jk}), \tag{3}$$

$$L_c = \sum_{jk} |R_{jk} - S_{jk}|. \tag{4}$$

The subscript  $c$  denotes CPS measures; the subscripts,  $j$  and  $k$ , denote the initial,  $y(i)$ , and final,  $y(i+1)$ , PS states, respectively. The value  $\lambda = 1$  results in  $d-1$  components of  $y(i+1)$  being redundant with those of  $y(i)$ ; we allow this redundancy to accommodate other data such as discrete points from two-dimensional maps. CPS measures have higher discriminating power than their nonconnected coun-

terparts. Indeed, we can prove<sup>42</sup> that these measures satisfy the following inequalities:  $\chi^2 \leq L$ ,  $\chi_c^2 \leq L_c$ ,  $L \leq L_c$ , and  $\chi^2 \leq \chi_c^2$ .

We call the quantities in Eqs. (1)–(4), phase space dissimilarity measures (PSDM). Their definitions show that PSDM can discriminate between different chaotic regimes. Such discrimination is not possible with TNM. The reason is rather simple: discrimination by TNM is based on a difference of averages, while discrimination via PSDM is based on averaging the absolute value of differences.

The disparate range and variability of these measures are difficult to interpret, especially for noisy data. We obtain a consistent means of comparison via renormalized dissimilarity measures (RDM),<sup>42,43</sup> which are defined by  $U(V) = |V_i - \bar{V}|/\sigma$ , as the number of standard deviations that the test case deviates from the base case mean.  $V$  denotes a dissimilarity measure from the set,  $V = \{L, L_c, \chi^2, \text{ and } \chi_c^2\}$ . We obtain the mean value,  $\bar{V}$ , of the dissimilarity measure by comparison among the  $B(B-1)/2$  unique combinations of the  $B$  base case cutsets, with a corresponding sample standard deviation  $\sigma$ . We subsequently compare each nonoverlapping test case cutset to each of the  $B$  base case cutsets, and obtain the corresponding average dissimilarity value,  $V_i$ , of the  $i$ th cutset for each dissimilarity measure. A statistically significant trend in the RDM indicates equipment degradation for failure forewarning.

The best choice of the parameter set,  $\{N, w, S, d, B, \lambda\}$ , depends not only on the system, but also on the specific data under consideration. We choose a “reasonable” value for the number,  $B$ , of base case cutsets,  $5 \leq B \leq 10$ , as a balance between a reasonably short quasistationary segment of “normal” dynamics and a sufficiently long internal for statistical significance. We find that the longest analysis window of  $N$  points is best, limited by the total length of the data. Our analysis proceeds as follows: (a) choose the parameter set,  $\{w, S, d, \lambda\}$ ; (b) compute the renormalized PS dissimilarities for the specific machine data; and (c) systematically search over the parameters,  $\{w, S, d, \lambda\}$ , to find the best forewarning indication.

Our previous work<sup>30–33</sup> found that RDM are sensitive measures of condition change, but that further improvements are needed to give an explicit indication of failure. Thus, we seek a more robust and specific end-of-life (EOL) forewarning. Extensive application of the PSDM approach<sup>33,34</sup> shows that all four of the PSDM display similar trends, as illustrated by the analysis of the machine data below. This observation suggests the definition of a composite measure,  $C_i$ , as the sum of the four renormalized PSDM for the  $i$ th dataset:

$$C_i = U(\chi^2) + U(\chi_c^2) + U(L) + U(L_c). \tag{5}$$

This composite measure is expected to be more robust than any one of the PSDM, while accurately indicating condition change. The end-of-life indication from this composite measure is then quantified as follows. We use contiguous, non-overlapping windows of  $C_i$  to obtain a least-squares straight-line fit:

$$y_i = ai + b. \tag{6}$$

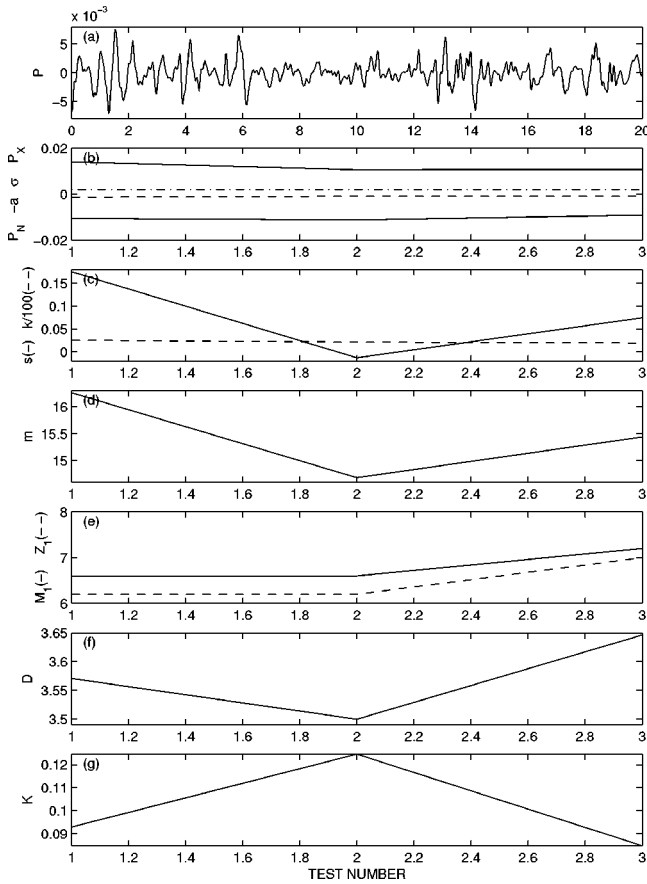


FIG. 1. Results for EPRI air-gap offset seeded fault: (a) vibrational power ( $P$ ) versus time (ms); (b) minimum ( $P_N$ ), negative of the absolute average deviation ( $-a$ ), standard deviation ( $\sigma$ ), and maximum ( $P_X$ ) of  $P$  for each test; (c) skewness ( $s$ ) and kurtosis ( $k$ ); (d) number of time steps per cycle ( $m$ ); (e) first minimum in the mutual information function ( $M_1$ ) and first zero in the autocorrelation ( $Z_1$ ); (f) correlation dimension ( $D$ ); and (g) Kolmogorov entropy ( $K$ ).

The window length of  $n=10$  values of  $C_i$  (and  $y_i$  below) is chosen consistent with the number of cutsets in each snapshot ( $B=10$ ). Other values of  $B$  give inferior indication of condition change. Next, the variance,  $\tilde{\sigma}^2$ , measures the variability of the  $C_i$  values about this straight-line fit:

$$\tilde{\sigma}^2 = \sum_i (y_i - C_i)^2 / (n - 1). \quad (7)$$

Finally,  $G$  measures the variability of next  $n$  values of  $C_i$  about an extrapolation of this straight-line:

$$G = \sum_i (y_i - C_i)^2 / \tilde{\sigma}^2. \quad (8)$$

Other fits (quadratic, cubic, and quartic) are inappropriate, because they extrapolate poorly outside the fitting window. The index,  $i$ , in Eqs. (6)–(8) runs over the  $B$  values of  $C_i$  and  $y_i$ .  $G$  has the form of a chi-squared statistic, but we do not use that notation to avoid confusion with the two  $\chi^2$  PSDM. A statistical test for  $G$  would involve (for example) the null hypothesis that deviations from the straight-line fit are normally distributed. Analysis of accelerated test data uses Eqs. (5)–(8) to extract both forewarning and an indication of failure onset. We present the results of this analysis next.

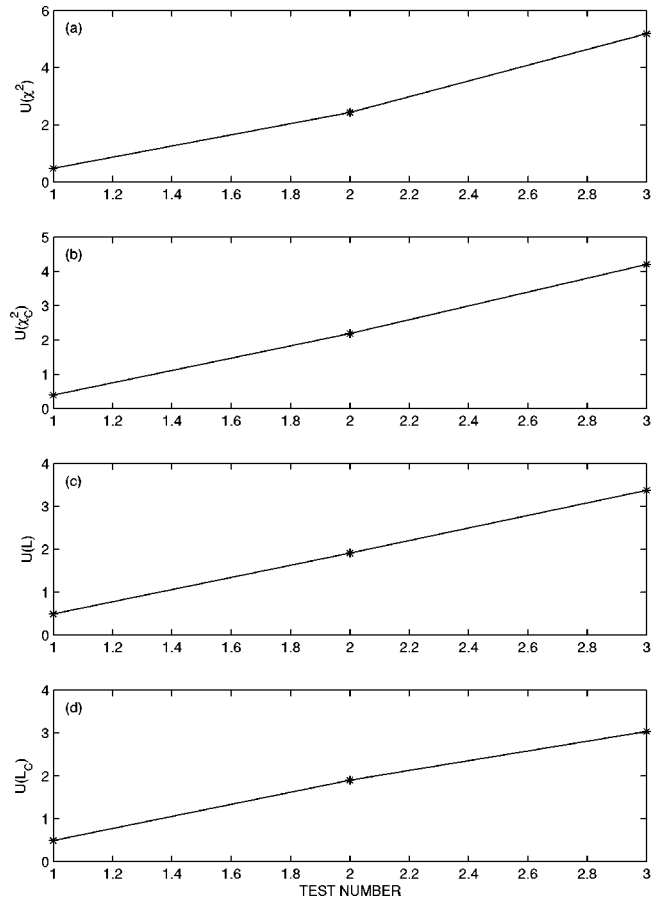


FIG. 2. Plots of the four nonlinear dissimilarity measures for the airgap-offset seeded-fault from vibration power with the following phase-space parameters:  $d=3$ ,  $S=3$ ,  $\lambda=11$ . Dataset #1 is for the nominal (no fault) state. Datasets #2–3 are for two different airgap-offset faults.

### III. ANALYSIS OF MACHINE DATA

Without a model, the “correct” choice of process-indicative data can be justified only *a posteriori*. As a practical matter, this choice is limited to measurable process variables. Moreover, the analyst’s choice must recognize that not all observables capture the same amount of information.<sup>38</sup> Typical machine data are triaxial acceleration,  $\mathbf{a}$ , and three-phase electrical current,  $I_i$ , and voltage,  $V_i$ . From these data, we calculate the instantaneous mechanical (vibration) or electrical power,  $P \propto \mathbf{a} \cdot \mathbf{f} \, dt$  or  $\sum_i I_i V_i$ , respectively. The use of vibration or electrical power is certainly not unique. Indeed, one component of acceleration (or current or voltage) may provide an adequate process-indicative signal to extract condition change. The use of power has the advantage that only one channel of data is analyzed, instead of several channels, to find the best signal for change discrimination. This paper presents details of the forewarning analysis via *vibration power*. Similar analyses of three-phase electrical power, and individual channels of current, voltage, acceleration, velocity, and torque are described in Refs. 32 and 34.

For this analysis, the datasets for each test in the sequence were concatenated into a single long dataset. We verify data quality by checking for: the proper number of data points, any intervals with unchanged signal amplitude,

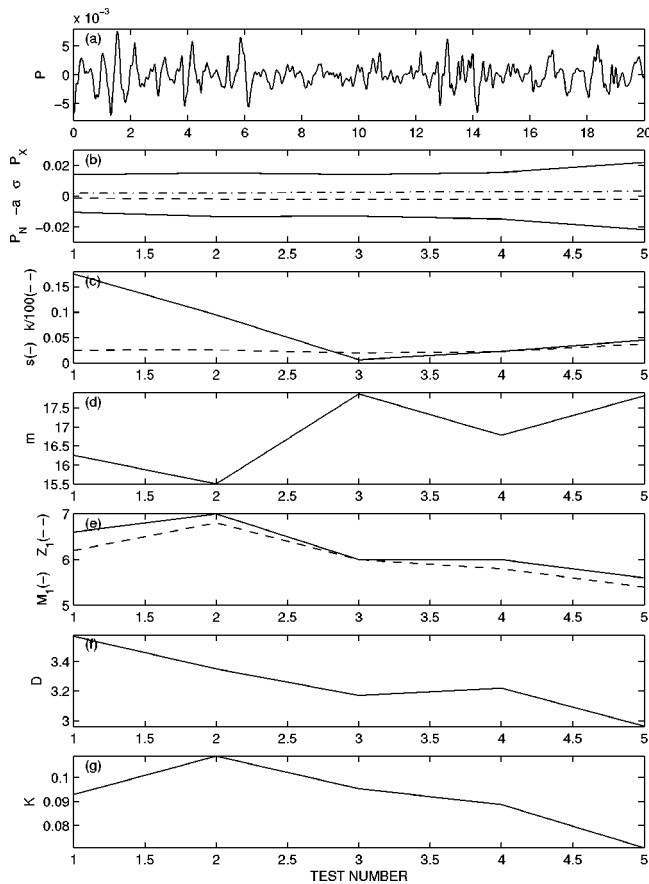


FIG. 3. Results for EPRI broken-rotor seeded fault: (a) vibration power ( $P$ ) versus time (ms); (b) minimum ( $P_N$ ), negative of the absolute average deviation ( $-a$ ), standard deviation ( $\sigma$ ), and maximum ( $P_X$ ) of  $P$  for each test; (c) skewness ( $s$ ) and kurtosis ( $k$ ); (d) number of time steps per cycle ( $m$ ); (e) first minimum in the mutual information function ( $M_1$ ) and first zero in the autocorrelation ( $Z_1$ ); (f) correlation dimension ( $D$ ); and (g) Kolmogorov entropy ( $K$ ).

adequate sampling rate, excessive periodic content, excessive noise, saturation at high or low limits as an indicator of improper data scaling, and consistent signal amplitude across datasets in the test sequence. The present analysis applies only to data that pass these quality tests.

The Electric Power Research Institute (EPRI) sponsored work on predictive maintenance for large motors, simulating common failures via seeded faults.<sup>56</sup> Present analyses use triaxial (vibration) acceleration data from inboard (IB) motor location, because all data from the outboard motor location failed the quality check. Data were recorded in 1.5-s snapshots at 40 kHz (60 000 points per dataset). Our analysis averages the measures over five subsets ( $B=5$ ) of 12 000 points.

**A. EPRI air-gap seeded fault**

One EPRI test<sup>56</sup> involved operator-imposed air-gap offsets in the rotor-stator alignment. The test bed was a three-phase, 800-HP sleeve-bearing, form-wound Allis Chalmers induction motor, rated at 4160 V and 100 A at 60 Hz with 10 poles, 94 copper rotor bars, 40 stator slots, running at a normal speed of 710 rpm. The first dataset of test sequence involves the motor running in its nominal state. Two differ-

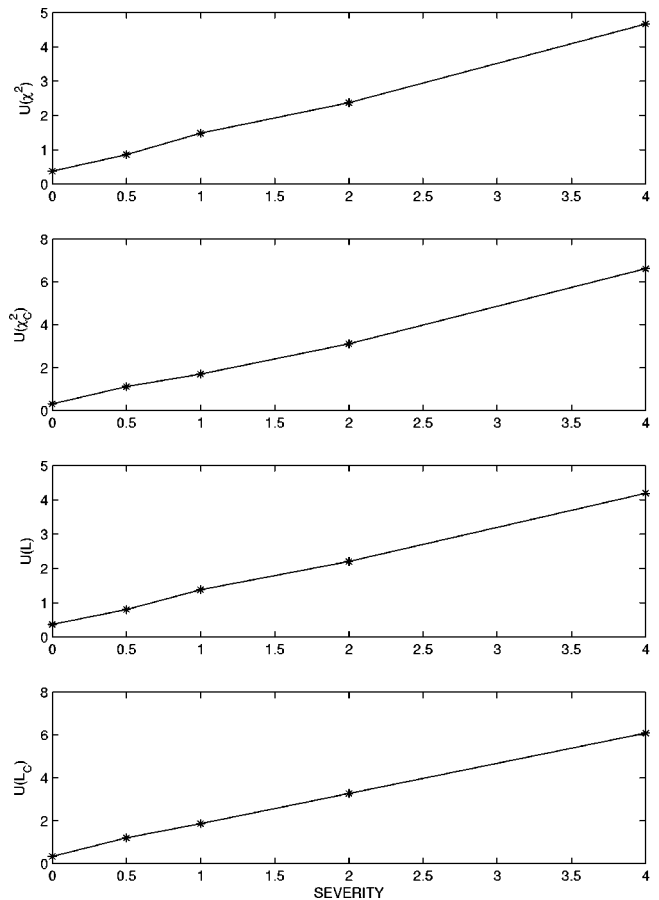


FIG. 4. Plots of the four nonlinear dissimilarity measures for the broken-rotor seeded-fault vibration power data versus fault severity (number of broken rotor bars). Dataset #1 is for the nominal (no fault) state. Dataset #2 is for the 50% cut in one rotor bar. Dataset #3 is for the 100% cut in one rotor bar. Dataset #4 is for two cut rotor bars. Dataset #5 is for four cut rotor bars. The PS reconstruction parameters are:  $d=3$ ,  $S=130$ , and  $\lambda=21$ .

ent air-gap offset seeded faults were then imposed via preinstalled jackscrews. The second dataset imposed a static inboard air-gap offset of 8 mils from the nominal value of 30 mils. The third dataset retained the first fault, and added a static outboard air-gap offset by 20% in the opposite direction from the inboard shift, resulting in the rotor being skewed relative to the stator. Figure 1(a) shows a 20 ms segment of vibration power data with complex, nonlinear features. The corresponding CSM [Figs. 1(b)–1(e)] and TNM [Figs. 1(e)–1(g)] do not provide a clear indication of the increasing severity of the seeded fault. In sharp contrast, Fig. 2 shows that all four PSDM rise linearly with increasing fault severity, yielding good change discrimination.

**B. EPRI rotor-bar seeded fault**

A second EPRI (Ref. 56) test involved operator-imposed partial or total cuts in the rotor bars. The test bed was the same Allis Chalmers motor. The test began with the motor running in its nominal state (first dataset), followed by progressively more severe broken rotor bars. The second dataset involved one rotor bar cross section cut 50% in half at the 11:00 position. The third dataset was for the same rotor bar now cut through 100%. The fourth dataset was for a second

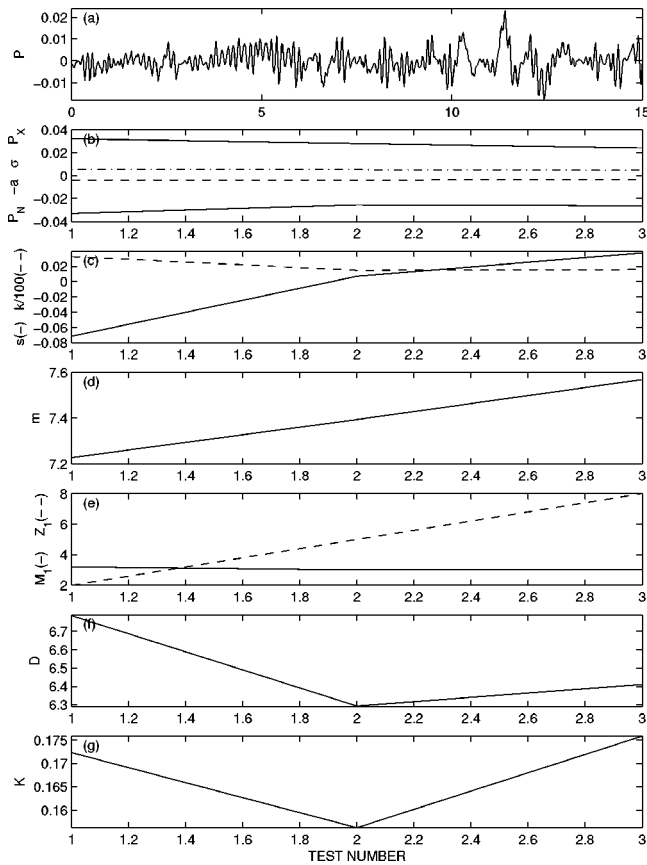


FIG. 5. Results for EPRI turn-to-turn seeded fault: (a) vibration power ( $P$ ) versus time (ms); (b) minimum ( $P_N$ ), negative of the absolute average deviation ( $-\sigma$ ), standard deviation ( $\sigma$ ), and maximum ( $P_X$ ) of  $P$  for each test; (c) skewness ( $s$ ) and kurtosis ( $k$ ); (d) number of time steps per cycle ( $m$ ); (e) first minimum in the mutual information function ( $M_1$ ) and first zero in the autocorrelation ( $Z_1$ ); (f) correlation dimension ( $D$ ); and (g) Kolmogorov entropy ( $K$ ).

rotor bar cut 100% at the 5:00 position, exactly  $180^\circ$  from, in addition to the first rotor failure. The fifth dataset was for two additional rotor bars cut adjacent to the original 11:00 bar, with one bar cut on each side of the original, yielding four bars completely open. The complete test sequence then captured an exponentially growing fault, from nominal operation, to  $\frac{1}{2}$ , to 1, to 2, to 4 broken rotor bars. Figure 3(a) shows a 20 ms segment of vibration power data with complex, nonlinear features. The corresponding CSM [Figs. 3(b)–3(e)] and TNM [Figs. 3(e)–3(g)] do not provide a clear indication of the exponentially-growing severity of the seeded fault. Figure 4 shows that all four PSDM rise linearly with the increasing fault severity, thus yielding good change discrimination.

**C. Analysis of turn-to-turn-short seeded fault data**

A third EPRI test<sup>56</sup> involved operator-imposed turn-to-turn shorts in a motor. The test bed was a three-phase, 500-HP, sleeve-bearing, form-wound General Electric induction motor, rated for 4000 V at 60 Hz, with 84 rectangular copper rotor bars, 6 poles, and 108 stator slots, running at a nominal speed of 1185 rpm. The first dataset was from the motor, running in its nominal state. A second dataset involved a

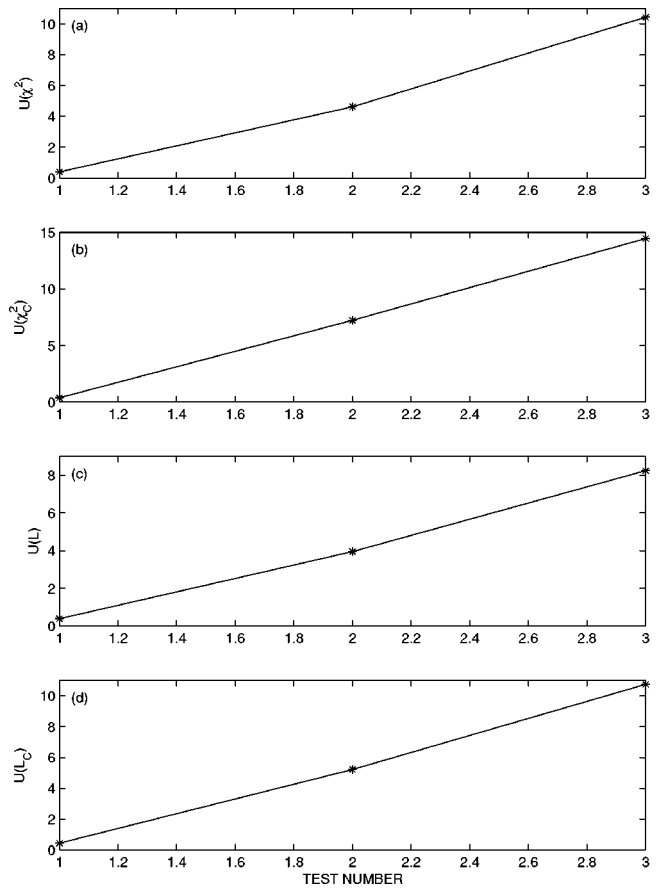


FIG. 6. Plots of the four nonlinear dissimilarity measures from the turn-to-turn short seeded-fault vibration power. Dataset #1 is for the nominal (no fault) state. Dataset #2 is for the 2.7-ohm short. Dataset #3 is for the 1.35-ohm short. The PS reconstruction parameters are:  $d=2$ ,  $S=6$ ,  $\lambda=57$ .

turn-to-turn (2.70-ohm) short by installing a large screw between two turns. A third dataset involved a more severe turn-to-turn (1.35-ohm) short by installing a smaller screw between two turns. The analysis sequence goes from largest turn-to-turn resistance (infinite resistance, corresponding to no short), to smaller (2.7 ohms), to smallest (1.35 ohms), corresponding to increasing severity in the fault. Figure 5(a) shows a 20 ms segment of vibration power data with complex, nonlinear features. The corresponding CSM [Figs. 5(b)–5(e)] and TNM [Figs. 5(e)–5(g)] show some consistency with the increasing severity of the seeded fault. The minimum ( $P_N$ ) rises and maximum ( $P_X$ ) falls [Fig. 5(b)] monotonically over the test sequence. Kurtosis decreases and skewness increases monotonically [Fig. 5(c)] over the test sequence. Linear increases occur in the average number of time steps per cycle [Fig. 5(d)] over a very narrow range (7.2–7.6), and the first zero in the autocorrelation function [Fig. 5(e)]. Figure 6 shows that all four PSDM rise linearly with the increasing fault severity, thus yielding good change discrimination.

**D. Analysis of gear-failure acceleration data**

The Pennsylvania State University (PSU) operates the Applied Research Laboratory,<sup>57</sup> including the Mechanical Diagnostics Test Bed (MDTB). A 30-HP, 1750-RPM, alter-

TABLE I. Summary of MDTB test results.

Run	Over-load	$\Delta\tau$ min	$r_{NEOL}$	$G_{NEOL}$	$r_{EOL}$	$G_{EOL}$	$T_{EOL}$ $T_{FAIL}$	$G_{ONSET}$	$T_{ONSET}$ $T_{FAIL}$	$T_{FAIL}$ h
36	2×	15	2.22	376	6.62	2493	0.985	244655	0.998	162.50
37	3×	1	1.79	333	8.07	2690	0.956	16284	0.996	8.55
38	3×	1	6.20	374	11.71	13486	0.938	48379	0.990	4.02
39	2×	1	2.32	853	3.89	5231	0.980	5231	0.980	8.60
39	3×	1	2.88	1151	29.03	33415	0.972	44552	0.994	8.60

nating current (ac), electric motor drives a gearbox, which is loaded by a 75-HP, 1750-RPM ac (absorption) motor. A digital vector drive unit controls the current to the absorption motor for torque variation up to 225 ft-lbs. The MDTB can test gear ratios from 1.2:1 to 6:1 in the 5–20 HP range at 2–5 times the rated torque of single and double reduction industrial gearboxes. The motors and gearbox are mounted and aligned on a bedplate, which is mounted on isolation feet to prevent vibration transmission to the floor. The shafts are connected with both flexible and rigid couplings. Torque limiting clutches on both sides of the gearbox prevent transmission of excessive torque during a gear jam or bearing seizure. Torque cells on both sides of the gearbox directly monitor the loads. The protocol for this accelerated failure test involves a break-in period at the nominal (1×) load (530 ft-lbs) for 1 h, followed by twice (2×) or three times (3×) the normal load, as shown in Table I, which also includes the time to failure ( $T_{fail}$ ). The EOL failures typically include pinion damage, broken teeth, and a sheared shaft. Ten-second snapshots of tri-axial accelerometer data were sampled at 52 kHz; see Table I for the interval ( $\Delta\tau$ ) between each snapshot. We convert the accelerometer data during the overload period into vibration power for this analysis. As before, the CSM and TNM show little if any failure forewarning,<sup>34</sup> so we do not show them here.

Figure 7 shows that all four PSDM rise systematically [Figs. 7(a)–7(d)] to provide failure forewarning. Indeed, the abrupt increase in all four PSDM at 160 h clearly forewarns of the imminent failure. We obtain this forewarning by quantifying significant deviations from the general trend via application of Eqs. (5)–(8). Chi-squared statistical tables give the corresponding value of  $G \leq 28.5$  for  $n=10$  degrees of freedom with a probability of one out of the 650 snapshots or ( $1/650 \sim 1.5 \times 10^{-3}$ ). However, we observe many instances of  $G > 28.5$  [solid curve in Fig. 7(f)], which arise from dynamical correlations in the accelerometer data, thus violating the requirement for independent, identically distributed samples.

Instead, we use  $G$  as a *relative* EOL measure. Although  $G$  varies erratically, we observe a systematic trend in the running maximum of  $G$ ,  $G_{max}$ , as shown by the dashed curve in Fig. 7(f), neglecting (for example) the first six  $G$ -values to avoid startup transients. This running maximum steadily increases in modest increments to 376 over the first 159.75 h of the test, while intermediate values of  $G$  fall well below the running maximum. Subsequently, a large increase occurs in  $G$  at 160 h, which produces a correspondingly large rise in  $G$  and therefore in  $G_{max}$ . The resulting jumps in  $G_{max}$  are quantified by the chain curve (---) in Fig. 7(f), as the ratio,

$r = (G_{max})_k / (G_{max})_{k-1}$ , of the current maximum in  $G$ ,  $(G_{max})_k$ , to the previous maximum in  $G$ ,  $(G_{max})_{k-1}$ .  $G$  rises to 2493 at 160 h, with a corresponding ratio,  $r=6.62$ , while the largest non-EOL ratio is  $r=2.22$  at 28.5 h. We find that the forewarning values of  $C_i$  across the various MDTB tests are not consistent, but that the values of  $G_{max}$  and  $r$  consistently do provide both forewarning of the failure and indication of the failure onset, as shown in Table I: (a) the largest non-EOL value of  $r$  ( $r_{NEOL}$ ) and the corresponding value of  $G$  ( $G_{NEOL}$ ); (b) values of  $r$  ( $r_{EOL}$ ) and  $G$  ( $G_{EOL}$ ) that indicate the EOL, and the matching time ( $T_{EOL}/T_{FAIL}$ ); (c) the

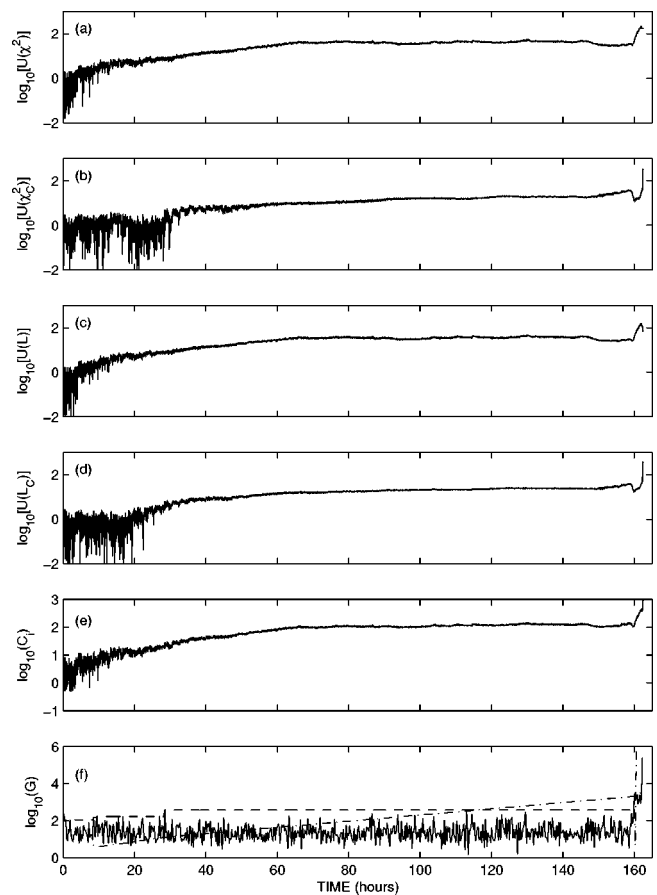


FIG. 7. Phase-space dissimilarity measures versus time for the MDTB accelerated failure test (run #36) from vibration power data: (a)–(d) the four renormalized PSDM; (e) composite measure,  $C_i$ , of the four PSDM; (f) end-of-life indicator,  $G$  (solid), running maximum of  $G$  (dashed), and ratio,  $r$ , of successive maxima (---) in  $G$ . Note that the vertical axis is the  $\log_{10}$  of the parameter is subplots (a)–(f), and that  $3 \log_{10}(r)$  is plotted in (f) for clarity. The phase-space parameters are  $S=274$ ,  $d=2$ , and  $\lambda=1$ , which are identical to those used in previous analysis (Ref. 32) to show forewarning consistency.

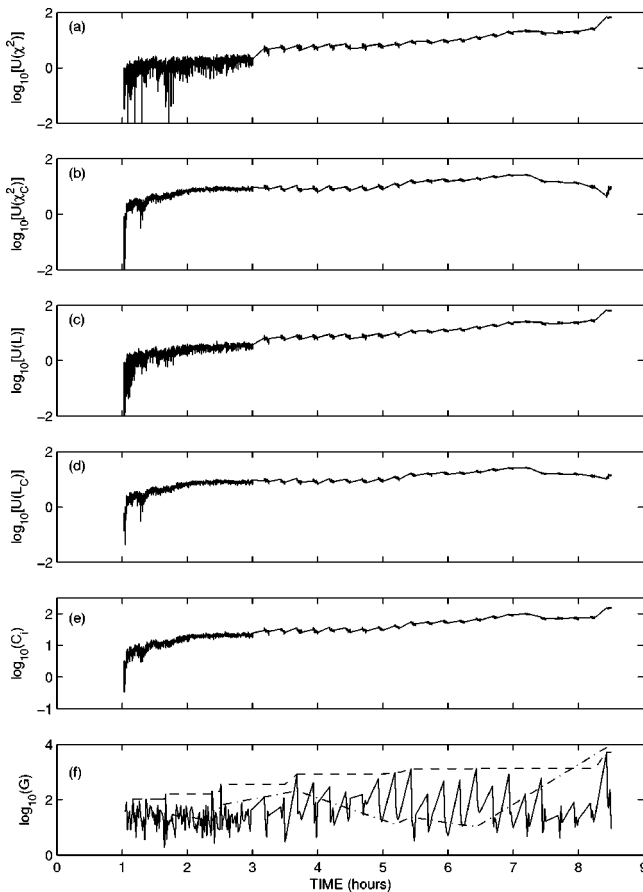


FIG. 8. Phase-space dissimilarity measures versus time for the MDTB accelerated failure test (run #39 2X portion) from vibration power data: (a)–(d) the four renormalized PSDM; (e) composite measure,  $C_i$ , of the four PSDM; (f) end-of-life indicator,  $G$  (solid), running maximum of  $G$  (dashed), and ratio,  $r$ , of successive maxima (– · –) in  $G$ . Note that the vertical axis is the  $\log_{10}$  of the parameter in subplots (a)–(f), and that  $3 \log_{10}(r)$  is plotted in (f) for clarity. The phase-space parameters are  $S=274$ ,  $d=2$ , and  $\lambda=1$ , which are identical to those used in previous analysis (Ref. 32) to show self-consistency.

value of  $G$  at failure onset ( $G_{\text{ONSET}}$ ) and the corresponding time ( $T_{\text{ONSET}}/T_{\text{FAIL}}$ ); and (d) the failure-endpoint time ( $T_{\text{FAIL}}$ ).

Table I also shows results for runs #37–38. The corresponding plots<sup>34</sup> are very similar to Fig. 7 and are not shown. Runs #36–38 have largest non-EOL values:  $r_{\text{NEOL}}=6.20$  and  $G_{\text{NEOL}}=376$ . The smallest EOL values are:  $r_{\text{EOL}}=6.62$  and  $G_{\text{EOL}}=2493$ . Thus, limits (for example) of  $r>6.4$  and  $G>1800$  provide EOL forewarning. Moreover, we find that the largest EOL value of  $G_{\text{EOL}}=13\,486$ , while the smallest failure-onset value is  $G_{\text{ONSET}}=16\,284$ . Thus, an intermediate value (for example) of  $G>15\,000$  distinguishes the EOL from failure onset forewarning. This approach gives quantitative limits for transitions from nominal operation (green light for “go” in a traffic signal metaphor), to forewarning of failure (yellow light for “caution”), and finally to failure onset (red light for “stop”).

MDTB Run #39 involves a different test protocol: a 1 h break-in period at nominal load ( $1\times$ ), followed by  $2\times$  load for 2 h, after which the load alternates between  $3\times$  and  $2\times$  loads for 10 and 5 min, respectively. Figures 8 and 9 show

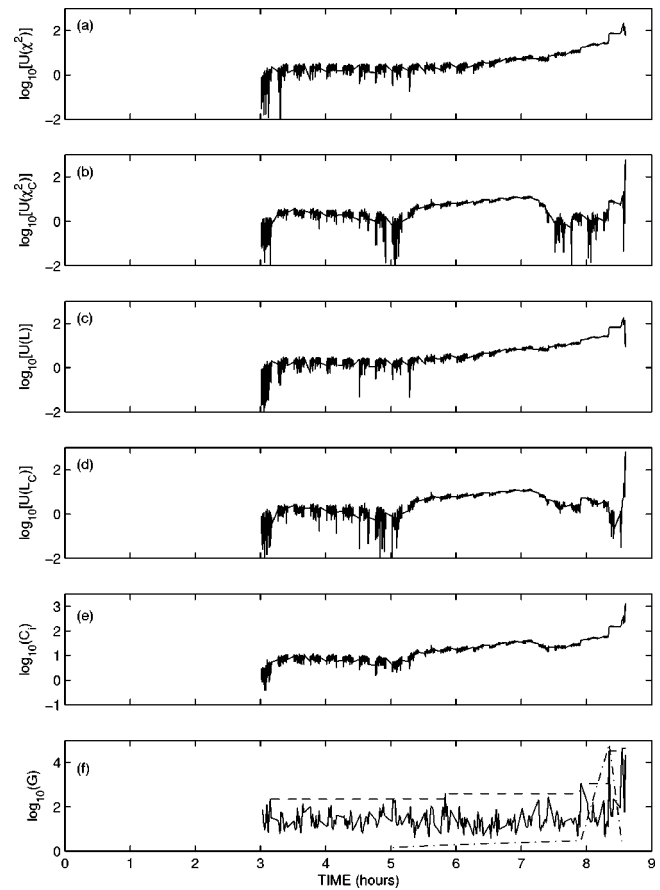


FIG. 9. Phase-space dissimilarity measures versus time for the MDTB accelerated failure test (run #39 3X portion) from vibration power data: (a)–(d) the four renormalized PSDM; (e) composite measure,  $C_i$ , of the four PSDM; (f) end-of-life indicator,  $G$  (solid), running maximum of  $G$  (dashed), and ratio,  $r$ , of successive maxima (– · –) in  $G$ . Note that the vertical axis is the  $\log_{10}$  of the parameter in subplots (a)–(f), and that  $3 \log_{10}(r)$  is plotted in (f) for clarity. The phase-space parameters are  $S=274$ ,  $d=2$ , and  $\lambda=1$ , which are identical to those used in previous analysis (Ref. 32) to show self-consistency.

run #39 PSDM for the  $2\times$  and  $3\times$  overload, respectively. The sawtooth features in each of the subplots correspond to the transition between  $2\times$  and  $3\times$  loads; the straight-line portion in Fig. 8 corresponds to the  $2\times$  segment in Fig. 9, and inversely. Run #39 seeks failure forewarning in the presence of load changes. Table I shows that the above limits for  $G$  and  $r$  also distinguish between the non-EOL (green) and EOL (yellow) states for the  $3\times$ -portion of this test, because the higher overload drives the failure. These limits do not apply to the  $2\times$  test, due to the reduced damage at the lower overload. Unsurprisingly, a different limit of  $G>38\,000$  (for example) distinguishes between the EOL and failure onset forewarnings, due to the change in test protocol. The green–yellow–red approach still applies for this test.

### E. Analysis of shaft-crack seeded fault

We analyzed additional PSU seeded-fault data with a progressively increasing depth of cut at the base of a motor-driven rotor blade. This test sequence simulates the growth of a crack in a turbomachine, which eventually causes failure. The rotor is driven at a fixed rotational speed by a frac-

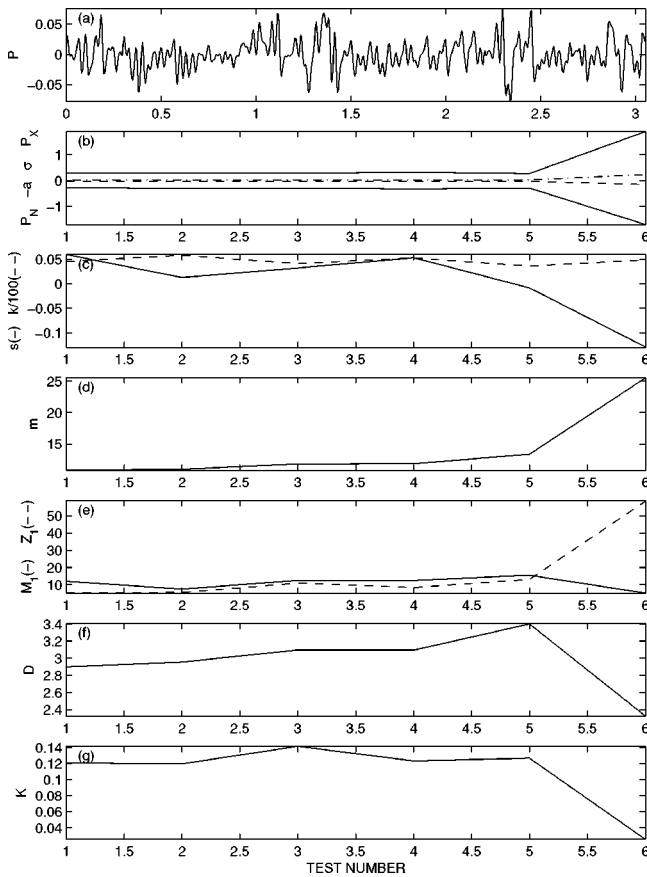


FIG. 10. Results for PSU turn-to-turn seeded generator fault: (a) vibration power ( $P$ ) versus time (ms); (b) minimum ( $P_N$ ), negative of the absolute average deviation ( $-a$ ), standard deviation ( $\sigma$ ), and maximum ( $P_X$ ) of  $P$  for each test; (c) skewness ( $s$ ) and kurtosis ( $k$ ); (d) number of time steps per cycle ( $m$ ); (e) first minimum in the mutual information function ( $M_1$ ) and first zero in the autocorrelation ( $Z_1$ ); (f) correlation dimension ( $D$ ); and (g) Kolmogorov entropy ( $K$ ).

tional horsepower dc motor that was made by Bodine Electric Company, with typical electrical values of 4 V and 2 A. Test data at each depth of cut were triaxial accelerations in three orthogonal directions on one bearing pillow block. The sequence test states were: (a) nominal operation with no cut, (b) successively deeper cuts through one of eight equiangularly spaced 5/8 in. diam shafts that were fixed perpendicular to the rotation axis of the motor-driven rotor. The cut depths range from 1/16 in. to 3/8 in. Figure 10 shows a resultant segment of vibration power [Fig. 10(a)], along with conventional statistical measures [Figs. 10(b)–10(e)], and traditional nonlinear measures [Figs. 10(e)–10(g)]. The magnitudes of minimum and maximum in vibration power [Fig. 10(b)] are constant, then rise abruptly for the deepest cut. The number of time steps per cycle [Fig. 10(d)] rises slowly and monotonically, also showing a large increase for the largest cut depth. None of the other measures in Fig. 10 show a consistent change over this test sequence. Figure 11 shows that all four PSDM rise monotonically by 100-fold as the cut depth increases from zero (baseline) to 3/8 in. These strong indications of change are in sharp contrast to the weak ones of Fig. 10.

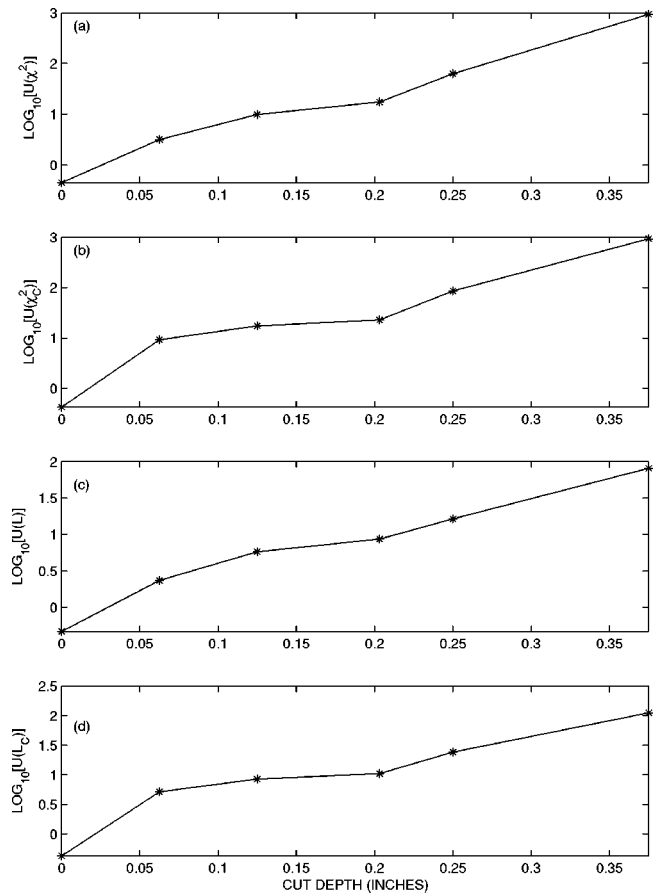


FIG. 11. The four PSDM versus cut depth for the shaft-crack seeded-fault from vibration power data. This result is for the best set of phase-space parameters:  $S=2$ ,  $d=4$ ,  $\lambda=23$ ,  $B=10$ , and  $N=100\,000$ .

IV. SUMMARY AND CONCLUSIONS

This work analyzes vibration power for comparison CSM, TNM, and PSDM as indicators of condition change due to various machine faults. Recent work by our team showed very similar results via analysis of electrical motor power, namely strong linear correlation of the PSDM with fault progression, and little if any correlation with the CSM and TNM.<sup>34</sup> Table II summarizes recent results for forewarning of seeded faults and accelerated failures in various machines and equipment. The CSM include minimum, maximum, average, sample standard deviation, skewness, kurtosis, average time steps per cycle, and first zero in the autocorrelation function. The TNM include first minimum in the mutual information function as a measure of decorrelation time, correlation dimension as a measure of complexity, and Kolmogorov entropy as a measure of information loss rate. PSDM are the  $\chi^2$  statistic and  $L_1$  distance between the time-delayed reconstructions of the PS-distribution functions on the discretized attractor.

PSDM show more consistent and better discriminating power for timely forewarning of failure or abnormal conditions, than either CSM or TNM. The reason for the improved performance of PSDM is rather simple. CSM and TNM compare averages, while PSDM are the sum over the absolute difference between the two PS states. In addition, the enhanced discrimination power facilitates use of PSDM

TABLE II. Summary of recent machine failure forewarning results.

Data provider	Equipment and type of failure	Diagnostic data	Reference
(1) EPRI (S)	800-HP electric motor: air-gap offset	motor power	32
(2) EPRI (S)	800-HP electric motor: broken rotor	motor power	32
(3) EPRI (S)	500-HP electric motor: turn-to-turn short	motor power	32
(4) Otero/Spain (S)	$\frac{1}{4}$ -HP electric motor: imbalance	acceleration	32
(5) PSU/ARL (A)	30-HP motor: overloaded gearbox	load torque	32
(6) PSU/ARL (A)	30-HP motor: overloaded gearbox	vibration power	32
(7) PSU/ARL (A)	30-HP motor: overloaded gearbox	vibration power	32
(8) PSU/ARL (S)	crack in rotating blade	motor power	32
(9) PSU/ARL (A)	motor-driven bearing	vibration power	32
(10) EPRI (S)	800-HP electric motor: air-gap offset	vibration power	present work
(11) EPRI (S)	800-HP electric motor: broken rotor	vibration power	present work
(12) EPRI (S)	500-HP electric motor: turn-to-turn short	vibration power	present work
(13) PSU/ARL (A)	30-HP motor: overloaded gearbox	vibration power	present work
(14) PSU/ARL (A)	30-HP motor: overloaded gearbox	vibration power	present work
(15) PSU/ARL (A)	30-HP motor: overloaded gearbox	vibration power	present work
(16) PSU/ARL (A)	30-HP motor: overloaded gearbox	vibration power	present work
(17) PSU/ARL (S)	crack in rotating blade	vibration power	present work

on noisier data. The sensitivity and robustness of PSDM depend both on the data quality and on the PS reconstruction parameters. Substantial improvements in both directions are possible from additional information about the underlying dynamical system. Indeed, (i) data quality can be improved by removal of (known) confounding artifacts from the signal, and (ii) reconstruction parameters can be chosen much closer to their optimal values. Without this information, one must resort to a trial and error procedure, which requires a search over a large subset of the parameter space to obtain the best indication of condition change.

Finally, we mention that this same approach provides forewarning and detection of various biomedical events. One line of recent research<sup>30,33,42–45,53–55,58</sup> shows forewarning of epileptic seizures from scalp EEG data. More recent biomedical applications<sup>33,59</sup> include forewarning of ventricular fibrillations from electrocardiogram (ECG) data, detection of sepsis onset from rat ECG, pig chest sounds to indicate greater breathing difficulty for a pneumothorax condition, and surface ECG data to forewarn of fainting. Success for these diverse applications provides confidence that this approach is useful for detecting condition change in nonlinear and chaotic processes for both machine and biomedical applications.

## ACKNOWLEDGMENTS

This work was supported by the U.S. Department of Energy (DOE) under the Nuclear Energy Research Initiative program, Award No. M0SF00-109 and NERI Project No. 2000-109, and by DOE's Division of Materials Science under the Office of Basic Energy Science. The Oak Ridge National Laboratory is managed for the U.S. Department of Energy by UT-Battelle, LLC, under Contract No. DE-AC05-00OR22725. We thank Dr. Jan Stein (Electric Power Research Institute) and Dr. Karl Reichard (Applied Research Laboratory at Pennsylvania State University) for providing data.

<sup>1</sup>NIST/ATP Workshop on Condition-Based Maintenance, [http://www.nist.gov/www/cbm/cbm\\_wp1.htm](http://www.nist.gov/www/cbm/cbm_wp1.htm).

<sup>2</sup>B. S. Berger, M. Rokni, and I. Minis, *Int. J. Eng. Sci.* **30**, 1433–1440 (1992).

<sup>3</sup>S. T. S. Bukkapatnam, A. Lakhtakia, and S. R. T. Kumara, *Phys. Rev. E* **52**, 2375–2387 (1995).

<sup>4</sup>S. T. Chiriacescu, *Stability in the Dynamics of Metal Cutting*, Studies in Applied Mechanics 22 (Elsevier, New York, 1990).

<sup>5</sup>G. Giacomelli and A. Politi, *Phys. Rev. Lett.* **76**, 2686–2689 (1996).

<sup>6</sup>I. Grabec, *Phys. Lett. A* **117**, 384–386 (1986).

<sup>7</sup>I. Grabec, in *Proceedings of the 8th International Acoustic Emissions Symposium* (Tokyo, Japan, 1986), pp. 87–93.

<sup>8</sup>I. Grabec, *Int. J. Mach. Tools Manuf.* **28**, 19–32 (1988).

<sup>9</sup>C. Hualing and D. Depei, "A new theoretical model of nonlinear chatter in cutting process," in *Proceedings of the 11th International Conference on Production Research (ICPR)*, 1991, pp. 932–936.

<sup>10</sup>K. Jemielniak and A. Widota, *Int. J. Mach. Tools Manuf.* **29**, 249–256 (1989).

<sup>11</sup>R. I. King, "Historical background," in *Handbook of High-Speed Machining Technology*, edited by R. I. King (Chapman and Hall, New York, 1985), Chap. 1.

<sup>12</sup>F. Koenigsberger and J. Tlustý, *Machine Tool Structures* (Pergamon, New York, 1970), Vol. 1.

<sup>13</sup>J. S. Lin and C. I. Weng, *Int. J. Mach. Tools Manuf.* **30**, 53–64 (1990).

<sup>14</sup>J. S. Lin and C. I. Weng, *Int. J. Mech. Sci.* **8**, 645–657 (1991).

<sup>15</sup>F. C. Moon, "Chaotic dynamics and fractals in material removal processes," in *Nonlinearity and Chaos in Engineering Dynamics*, edited by J. M. T. Thompson and S. R. Bishop (Wiley, New York, 1994), Chap. 2.

<sup>16</sup>L. Qu, A. Xie and X. Li, *Mech. Mach. Theory* **28**, 699–713 (1993).

<sup>17</sup>G. Stépán, *Retarded Dynamical Systems: Stability and Characteristic Functions*, Pitman Research Notes in Mathematics (Wiley, New York, 1989), Vol. 210.

<sup>18</sup>J. Tlustý, "Machine dynamics," in *Handbook of High-Speed Machining Technology*, edited by R. I. King (Chapman and Hall, New York, 1985), Chap. 3.

<sup>19</sup>J. Tlustý and F. Ismail, *Ann. CIRP* **30**, 299–304 (1981).

<sup>20</sup>J. Tlustý and M. Poláček, in *Proceedings of the 9th MTDR Conference* (Pergamon, Oxford, 1968), pp. 521–570.

<sup>21</sup>S. A. Tobias, *Machine-Tool Vibration* (Wiley, New York, 1965).

<sup>22</sup>Y. Ueda, H. Ohta, and H. B. Stewart, *Chaos* **4**, 75–83 (1994).

<sup>23</sup>D. B. Welbourn and J. D. Smith, *Machine-Tool Dynamics: An Introduction* (Cambridge University Press, Cambridge, 1970), Chaps. 4–5.

<sup>24</sup>D. W. Wu and C. R. Liu, *J. Eng. Ind.* **107**, 107–111 (1985).

<sup>25</sup>D. W. Wu and C. R. Liu, *J. Eng. Ind.* **107**, 112–118 (1985).

<sup>26</sup>S. Smith and J. Tlustý, *Ann. CIRP* **41**, 433–436 (1992).

<sup>27</sup>R. Teltz and M. A. Elbestawi, *Trans. ASME* **115**, 122–132 (1993).

<sup>28</sup>L. M. Hively, N. E. Clapp, and C. S. Daw, "Nonlinear analysis of ma-

- ching data," ORNL/TM-13157 (Oak Ridge National Laboratory, Oak Ridge, TN, January 1996).
- <sup>29</sup> L. M. Hively, V. A. Protopopescu, N. E. Clapp, and C. S. Daw, "Prospects for chaos control of machine tool chatter," ORNL/TM-13283 (Oak Ridge National Laboratory, Oak Ridge, TN, June 1998).
- <sup>30</sup> L. M. Hively, "Data-driven nonlinear technique for condition monitoring," in *Proceedings of the Maintenance and Reliability Conference* (University of Tennessee, Knoxville, TN, 1997), Vol. 1, pp. 16.01–16.10.
- <sup>31</sup> L. M. Hively, V. A. Protopopescu, M. Maghraoui, and J. W. Spencer, "Annual Report for NERI Proposal #2000-0109 on forewarning of failure in critical equipment at next-generation nuclear power plants," ORNL/TM-2001/195 (Oak Ridge National Laboratory, Oak Ridge, TN, September 2001).
- <sup>32</sup> L. M. Hively and V. A. Protopopescu, "Forewarning of failure in critical equipment at next generation nuclear power plants," ORNL/TM-2002/183 (Oak Ridge National Laboratory, Oak Ridge, TN, December 2002).
- <sup>33</sup> L. M. Hively and V. A. Protopopescu, "Detection of changing dynamics in physiological time series," in *Proceedings of the Nuclear Mathematical Computational Science* (American Nuclear Society, LaGrange, IL, 2003).
- <sup>34</sup> L. M. Hively, V. A. Protopopescu, K. M. Reichard, and K. P. Maynard, "Failure forewarning in NPP equipment—NER12000-109 final project report," ORNL/TM-2003/222 (Oak Ridge National Laboratory, Oak Ridge, TN, 2003).
- <sup>35</sup> C. Caravati, F. Delogu, G. Cocco, and M. Rustici, *Chaos* **9**, 219–226 (1999).
- <sup>36</sup> G. Manal, F. Delogu, and M. Rustici, *Chaos* **12**, 601–609 (2002).
- <sup>37</sup> F. Pfeiffer, *Chaos* **4**, 693–705 (1994).
- <sup>38</sup> C. Letellier, J. Maquet, L. Le Sceller, G. Gouesbet, and L. A. Aguirre, *J. Phys. A* **31**, 7913–7927 (1998); C. Letellier and L. A. Aguirre, *Chaos* **12**, 549 (2002).
- <sup>39</sup> J. P. Eckmann and D. Ruelle, *Rev. Mod. Phys.* **57**, 617–655 (1985).
- <sup>40</sup> H. D. I. Abarbanel, *Analysis of Observed Chaotic Data* (Springer, New York, 1996).
- <sup>41</sup> A. Cover, J. Reneke, S. Lenhart, and V. Protopopescu, *Math. Models and Meth. in Appl. Sci.* **7**, 823–845 (1997).
- <sup>42</sup> L. M. Hively, V. A. Protopopescu, and P. C. Gailey, *Chaos* **10**, 864–875 (2000).
- <sup>43</sup> V. A. Protopopescu, L. M. Hively, and P. C. Gailey, *J. Clin. Neurophysiol.* **18**, 223–245 (2001).
- <sup>44</sup> L. M. Hively, N. E. Clapp, C. S. Daw, and W. F. Lawkins, "Nonlinear analysis of EEG for epileptic events," ORNL/TM-12961 (Oak Ridge National Laboratory, Oak Ridge, TN, 1995).
- <sup>45</sup> L. M. Hively, P. C. Gailey, and V. A. Protopopescu, *Phys. Lett. A* **258**, 103–114 (1999).
- <sup>46</sup> *Handbook of Mathematical Functions*, edited by M. Abramowitz and I. A. Stegun (U.S. Government Printing Office, Washington, D.C., 1965).
- <sup>47</sup> H. Kantz and T. Schreiber, *Nonlinear Time Series Analysis* (Cambridge University Press, Cambridge, 1997).
- <sup>48</sup> C. E. Shannon and W. Weaver, *The Mathematical Theory of Communication* (University of Illinois Press, Urbana, 1949).
- <sup>49</sup> A. M. Fraser and H. L. Swinney, *Phys. Rev. A* **33**, 1134–1140 (1986).
- <sup>50</sup> F. Takens, *Lect. Notes Math.* **1125**, 99–106 (1984).
- <sup>51</sup> J. C. Schouten, F. Takens, and C. M. van den Bleek, *Phys. Rev. E* **50**, 1851–1861 (1994).
- <sup>52</sup> J. C. Schouten, F. Takens, and C. M. van den Bleek, *Phys. Rev. E* **49**, 126–129 (1994).
- <sup>53</sup> P. C. Gailey, L. M. Hively, and V. A. Protopopescu, "Robust detection of dynamical change in scalp EEG," in *Proceedings of the Fifth Experimental Chaos Conference*, June 28–July 1, 1999, Orlando, Florida.
- <sup>54</sup> L. M. Hively, P. C. Gailey, and V. A. Protopopescu, "Sensitive measures of condition change in EEG data," in *Proceedings of the International Workshop: "Chaos in Brain?"* Bonn, Germany, 10–12 March 1999, edited by K. Lehnertz *et al.* (World Scientific, Singapore, 2000), pp. 333–336.
- <sup>55</sup> V. Protopopescu, L. M. Hively, and P. C. Gailey, "Robust forewarning of dynamical change from single channel scalp EEG data," in *Proceedings of the 18th Energy Symposium on Energy Science*, May 15–16, 2000, Argonne, IL, pp. 137–145.
- <sup>56</sup> Electric Motor Predictive Maintenance Program, EPRI, Palo Alto, CA (1999) TR-108773-V2.
- <sup>57</sup> [http://muri.arl.psu.edu/shared\\_data\\_repository.html](http://muri.arl.psu.edu/shared_data_repository.html)
- <sup>58</sup> L. M. Hively and V. A. Protopopescu, *IEEE Trans. Biomed. Eng.* **50**, 584–593 (2003).
- <sup>59</sup> L. M. Hively, V. A. Protopopescu, and N. B. Munro, "Detection of changing dynamics in physiological time series for biomedical event forewarning," *Biomedical Engineering Society Conference* (Biomedical Engineering Society, Nashville, TN, 2003).